THESIS FOR THE DEGREE OF DOCTOR OF PHILOSOPHY IN SOLID AND STRUCTURAL MECHANICS

Multiphysics Modelling and Calibration of Structural Battery Electrodes and Full Cells

Carl Larsson

Department of Mechanical Engineering
Chalmers University of Technology
Gothenburg, Sweden, 2026

Multiphysics Modelling and Calibration of Structural Battery Electrodes and Full Cells
Carl Larsson
ISBN 978-91-8103-429-5

Technical Report No. 5886
ISSN 0346-718X
This thesis has been prepared using LaTeX.

Department of Mechanical Engineering
Division of Computational Mechanics and Materials Engineering
Chalmers University of Technology
SE-412 96 Gothenburg, Sweden
Phone: +46 (0)31 772 1000
www.chalmers.se

Printed by Chalmers Reproservice
Gothenburg, Sweden 2026

Abstract

As the demand for lightweight energy storage solutions intensifies, structural battery composites have emerged as a promising technology merging electrochemical capacity with mechanical load carrying capability. Unlike conventional systems, where energy storage is typically implemented as battery packs that add mass, structural batteries integrate this function directly into structural elements. The multifunctionality is achieved by utilizing carbon fibres as both the primary structural reinforcement and as active electrode material. To facilitate ion transfer between the electrodes, while maintaining structural integrity, the fibres are embedded in a Structural Battery Electrolyte (SBE)—a bicontinuous material consisting of a porous polymer skeleton and a liquid electrolyte.

The first part of this thesis studies the constitutive modelling and characterization of the structural negative electrode and its constituents. A concentration-dependent constitutive model is developed for the carbon fibres to account for the significant swelling and the evolution of elastic moduli induced by lithium-ion insertion under finite deformations. This is complemented by a continuum porous media representation of the SBE, which utilizes a visco-hyperelastic model for the solid skeleton and incorporates the principle of effective stress to capture the time-dependent coupling between deformation and pore fluid pressure. To accurately analyze the complex internal stress states on the microscale, governed by fibre expansion, SEM micrograph informed microstructures are generated. By integrating the developed constitutive models for both the fibre and the SBE these representative volume elements, the framework resolves the local mechanical interactions between the swelling fibres and the surrounding matrix in the negative electrode during lithiation.

The second part of the thesis develops a coupled computational framework for structural battery full cells. The model is calibrated against experimental charge-rest-discharge voltage profiles, including different charge rates. A sensitivity study is conducted to quantify the contribution of the calibrated parameters to the simulated voltage profiles. The framework is further developed and utilized to characterize the coupled potential-strain response, where an integrated experimental-computational study concludes that the carbon fibres in the negative electrode is the primary contributor to electric potential shifts during mechanical loading. This finding demonstrates an inherent sensing functionality within the structural electrode and validates the multifunctionality of the full cell.

Keywords: Structural Batteries, FEM, Multiphysics Modelling, Computational Homogenization, Experimental Characterization, Carbon Fibre Composite, Multifunctional Materials

Preface

The work in this thesis was carried out from February 2022 to May 2026 in the Division of Computational Mechanics and Materials Engineering, Department of Mechanical Engineering, Chalmers University of Technology. The research was financially supported by the US Air Force through the EOARD Award No. FA8655-21-1-7038 and FA8655-25-1-7049, and the Office of Naval Research through Contract No. N62909-22-1-2035; all funders are gratefully acknowledged.

Acknowledgements

I would like to start by thanking my main supervisor, Professor Leif Asp, for your excellent support during my time at Chalmers; this thesis would quite literally have carried no weight without your guidance. Moreover, I would like to extend my gratitude to Professor Fredrik Larsson for sharing your expertise in computational mechanics and for being immensely patient with me. My sincere thanks also go to Assistant Professor Johanna Xu and Professor Kenneth Runesson for your excellent co-supervision and for always pointing me in the right direction.

To my colleagues and friends at Chalmers, thank you for making the office feel like a second home. From the coffee breaks to the weekend activities, you made the journey toward a PhD very enjoyable. I would also like to thank Professor Ramesh Talreja for welcoming and hosting me at Texas A&M University. To the PhD students in College Station who turned a research stay into a collection of lasting memories—thank you!

Finally, to my family and friends, thank you for all the support. A special thanks goes to my Dad for inspiring me to pursue this degree and for his encouragement, which kept me going when the simulations wouldn't converge. And to my partner, Amanda, thank you for your endless support and for reminding me that there is life beyond carbon fibres. In addition to those mentioned above, thanks to everyone else who contributed to this journey.

List of publications

This thesis consists of work presented in the following papers:

A **Effects of lithium insertion induced swelling of a structural battery negative electrode**
Carl Larsson, Fredrik Larsson, Johanna Xu, Kenneth Runesson, Leif E. Asp
Composites Science and Technology, 2023, 110299

B **Poro-mechanical analysis of a structural battery electrolyte: experimental study and model calibration**
Carl Larsson, Fredrik Larsson, Ruben Tavano, Johanna Xu, Kenneth Runesson, Leif E. Asp
Mechanics of Materials, 2026, 105632

C **Mechanical response of the negative electrode in structural batteries with nonuniform microstructure**
Carl Larsson, Ramesh Talreja, Fredrik Larsson, Richa Chaudhary, Amanda Persdotter, Leif E. Asp
Submitted

D **Electro-chemo-mechanical modelling of structural battery composite full cells**
Carl Larsson, Fredrik Larsson, Johanna Xu, Kenneth Runesson, Leif E. Asp
npj Computational Materials, 2025, 141

E **Electro-chemo-mechanical coupling in structural lithium-ion batteries: Experimental findings and numerical modelling**
Rauan Al-Emrani, **Carl Larsson**, Clara Dahlberg, Fredrik Larsson, Leif E. Asp, Johanna Xu
Composites part B: Engineering, 2026, 113286

The appended papers were prepared in collaboration with the co-authors. The author of this thesis was responsible for the major progress of the work in the papers, i.e. took part in formulating theory, developed the numerical implementations, carried out numerical simulations and prepared the manuscripts. In **Paper E**, the first authorship is shared. The author of this thesis worked with development of the model, development of numerical implementations, carried out simulations related to parameter identification, preparation of the numerical method section and results related to parameter identification in the manuscript.

Other publications by the author, not included in this thesis, are:

Advancing structural battery composites: robust manufacturing for enhanced and consistent multifunctional performance
Mohammad Siam Siraj, Samia Tasneem, David Carlstedt, Shanghong Duan, Marcus Johansen, **Carl Larsson**, Johanna Xu, Fang Liu, Fredrik Edgren, Leif E Asp
Advanced Energy and Sustainability Research, 2023, 2300109

Multiscale modeling framework for estimating and calibrating the mechanical response of Li-ion battery cell components
David Carlstedt, Amit Chetry, **Carl Larsson**, Ankeet Mohan Purantagi, Peter Gustavsson, Fredrik Larsson, Leif E. Asp
Journal of Power Sources, 2025, 238237

Contents

1 Introduction

1.1 Background

Structural battery composites are multifunctional materials that combine electrochemical energy storage and mechanical load carrying capability within a single system. In conventional devices that are powered with batteries, these functions are separated. In addition to the load carrying structure, energy storage is typically implemented as a separate battery pack, which adds mass and volume and imposes design constraints. Structural battery composites based on lithium ion battery technology, in contrast, are intended to be integrated directly into the structure of the system they power, allowing structural elements to store and deliver electrochemical energy [1–6]. This integration has the potential to reduce or eliminate the need for dedicated battery packs, enabling lighter and more compact system architectures and increasing overall efficiency. Recent breakthroughs have established the realization of structural battery architectures that use carbon fibres as negative electrode material, achieving high multifunctional efficiency [7–10]. Subsequent efforts by Chaudhary et al. [11, 12] have refined this concept through the development of cathode coatings to allow the use of carbon fibres in the positive electrode as well. An illustration of the all-fibre structural battery architecture is shown in Figure 1.1. The electrodes are embedded in a nano-porous Structural Battery Electrolyte (SBE) matrix.

The motivation for structural battery research is particularly strong in the transport sector, where electrification is advancing rapidly. Sales of battery electric vehicles and heavy-duty electric vehicles continue to increase, while vehicle mass remains a key factor influencing energy consumption and driving range [13, 14]. Integrating structural batteries while maintaining overall vehicle mass has the potential to increase driving range by up to 70 % [15].

A key constituent of structural battery composites is the multifunctional carbon fibres with lithium storage capability, which simultaneously provide electrical conductivity and mechanical reinforcement [16–21]. In this role, the fibres replace conventional negative electrode materials, such as graphite, used in traditional batteries. Studies on the effects of lithium insertion into carbon fibres, known as lithiation, have demonstrated that lithiation induces an expansion of the fibre [22]. Further investigations of carbon fibre lithiation conducted by Duan et al. [23] demonstrate that the fibre expansion can reach levels as high as 6.6 % in the radial direction and 0.89 % in the axial direction upon full lithiation. Moreover, it has been observed that the elastic moduli of the fibre are significantly affected, the transverse (radial) modulus increases by 107 %, while the longitudinal modulus experiences a decrease by 12 %. Consequently, operating the structural battery results in substantial changes in the internal stress state and stiffness properties of the composite. The same coupling also leads to a response when a mechanical load is applied to lithiated (and partially lithiated) carbon fibres, resulting in a change in electric potential. This phenomenon, often referred to as stress-driven diffusion or the Piezo-Electro-Chemical Transducer effect (PECT), represents the interaction of electrochemistry and mechanics [9, 24–26].

The SBE is a bi-phasic matrix material consisting of a solid phase that enables mechanical load transfer and a liquid phase that facilitates ionic transport between the electrodes during charge and discharge [27–31]. An illustration of its nano-porous structure is shown in Figure 1.1b. A key design requirement for the SBE is its ability to deform reliably without fracture when subjected to mechanical loading arising from carbon fibre expansion during lithiation, as well as from externally applied mechanical loads. Recent measurements by Pipertzis et al. [32] indicate an almost three-fold increase in effective ionic conductivity after ten lithiation–delithiation cycles. This observation suggests that significant morphological changes may occur within the SBE as the fibres undergo repeated expansion and contraction. One possible explanation is that damage or rearrangement of the solid phase creates additional free volume, thereby facilitating ionic transport. Understanding the solid-fluid interaction, mechanical and electrochemical response of the SBE under such coupled loading conditions is therefore essential.

Furthermore, the positive electrode consists of active lithium iron phosphate $LiFePO_4$ (LFP) material and conductive particles adhered to an aluminium foil or deposited on carbon fibres [10, 11, 33]. Previous structural battery concepts employed commercially available LFP slurry cast onto aluminium foil, largely following conventional lithium-ion battery electrode architectures. In contrast, the current state of the art is based on LFP deposited directly onto carbon fibres, enabling the fibres to function simultaneously as current collectors and load bearing constituents.

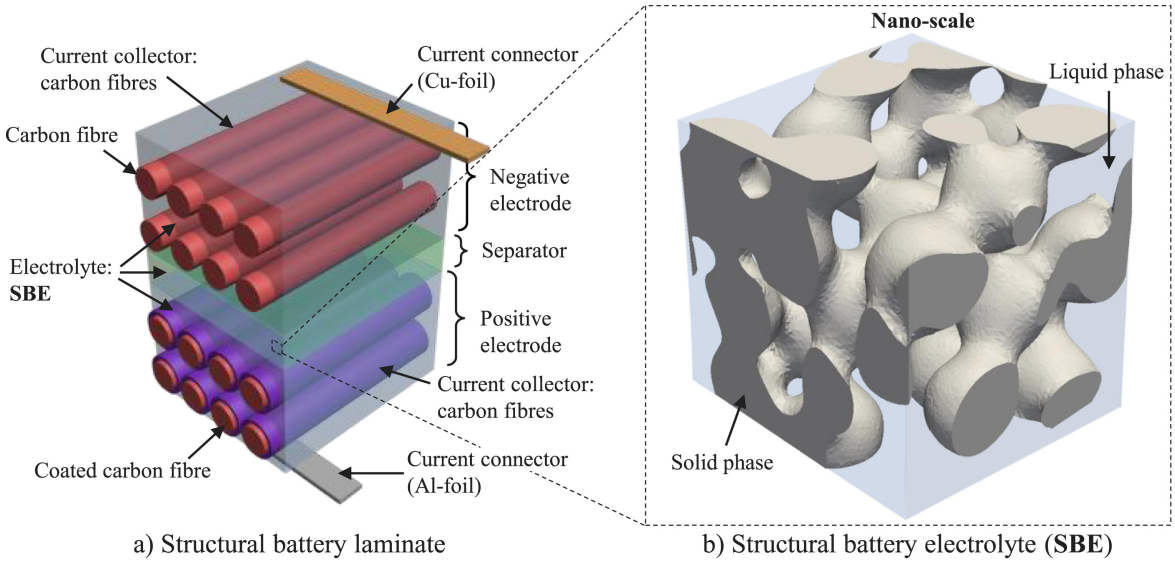

Figure 1.1: a) Schematic illustration of the laminated structural battery full cell. b) Numerical realization of the nano-porous structural battery electrolyte (SBE). From Carlstedt et al. [34].

To support the development of structural batteries, computational modelling has been extensively addressed by Carlstedt et al. [34–37], who presented a coupled thermo-electro-chemo-mechanical framework. These models emphasize coupling of fields, including the PECT effect. The proposed framework employ linearized (small strain) kinematics, linearized reaction kinetics and was formulated for a half-cell configuration, consisting of a carbon fibre electrode paired with a lithium metal reference electrode.

From a modelling perspective, the all-fibre structural battery full cell architecture illustrated in Figure 1.1a remains unexplored. A significant difficulty arises from the positive electrode, where active LFP particles span length scales from nanometres to micrometres. Resolving these particles explicitly within a battery scale finite element model would require direct numerical simulations that are computationally infeasible, in particular for nano-sized particles [38]. To address this challenge, homogeneous, macroscale models of electrodes and battery cells are employed, wherein the heterogeneous microstructure is represented through effective, averaged material properties [39–46]. While this approach enables simulations at the cell level, it inevitably leads to a loss of information regarding the spatial distribution of reaction sites and the local particle–electrolyte reaction kinetics. Moreover, the effective interface is are not directly measurable and must, instead, be determined through numerical and physical macroscopic experiments. Given these modelling challenges, it is essential to develop modelling techniques that can accurately predict the multifunctional response of structural battery components.

1.2 Aim and scope of research

The overall aim of this thesis is to advance the understanding of the coupled mechanical and electrochemical processes governing the behaviour of structural battery electrodes, and to develop improved computational modelling techniques capable of predicting their mechanical and electrochemical response. Emphasis is placed on the formulation of computational models for both structural battery half-cells and full cells, and on anchoring these models to experimental observations through model calibration. The research aims are summarized in the sub-goals presented below.

Sub-goals adressing the mechanical properties of the *structural negative electrode*:

i To characterize the resulting mechanical response of the carbon fibres during lithium insertion, based on experimental understanding of how the effect of lithium insertion affects expansion and elastic moduli. This involves the development of a computational model formulated within a finite strain setting that accounts for concentration dependent moduli as well as anisotropic expansion.

ii To propose and calibrate a constitutive model for the structural battery electrolyte matrix material. This objective focuses on capturing the coupled solid-fluid interaction within the SBE and validating the model's predictive capability against experimental data.

iii To develop a micromechanical model based on SEM-image informed Representative Volume Element (RVE) reconstructions for the structural negative electrode. These statistically representative domains, are used to investigate the complex internal stress states and the composite expansion induced by the lithiation of the carbon fibres.

Sub-goals related to electro-chemo-mechanical coupled processes in the *structural battery full cell*:

iv To develop a fully coupled electro-chemo-mechanical model for a structural battery composite full cell. This objective involves identifying key material parameters by calibrating the model against experimental charge-rest-discharge voltage profiles, followed by a sensitivity analysis to quantify the influence of these parameters on the macroscopic cell performance over varying operating rates.

v To further refine the electro-chemo-mechanical model with a specific focus on characterizing the coupled potential-strain response for a structural battery full cell. This objective involves the calibration of material parameters against experimental data to accurately capture and predict the variations in electric potential induced by external mechanical loading.

2

Mechanical considerations of the structural negative electrode and its constituents

2.1 The structural negative electrode

The negative electrode is composed of two primary constituents; the carbon fibres and the surrounding structural battery electrolyte (SBE) matrix. At the microscale, the carbon fibres are explicitly resolved as discrete entities, whereas the SBE is represented as a continuum with effective properties. Consequently, the computational domain of the fibres is defined as $\Omega^{\mathrm{f}} = \bigcup_{i=1}^{n} \Omega_i^{\mathrm{f}}$, and the electrolyte domain is denoted by Ω^{SBE}, these domains constitute the negative electrode domain $\Omega_{\square} = \Omega^{\mathrm{f}} \cup \Omega^{\mathrm{SBE}}$ shown in Figure 2.1.

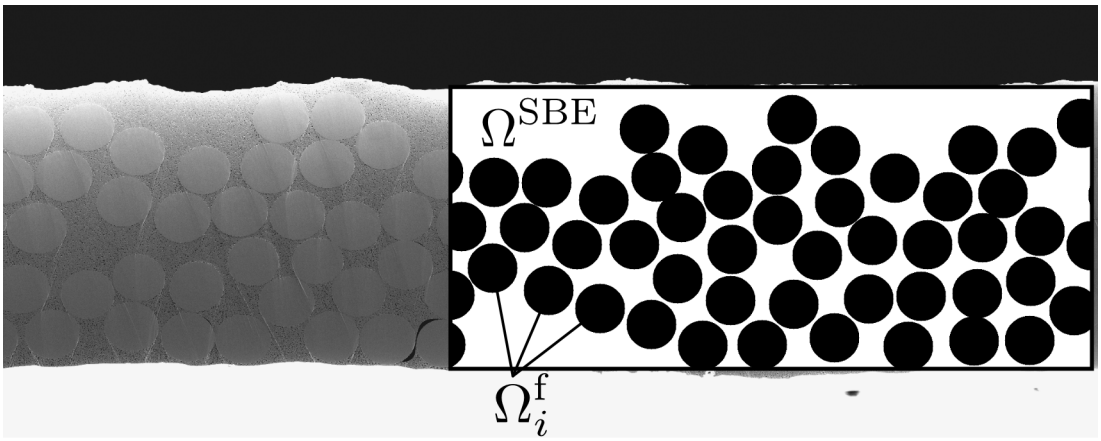

Figure 2.1: SEM image of the negative electrode, as well as an illustration of a computational domain $\Omega_{\square}$.

In **Paper A**, the structural negative electrode is represented in finite strain setting where model development is emphasized for the carbon fibres. Finite strains are required to predict geometrical changes as well as to accurately predict the internal stress-state in the SBE upon carbon fibre expansion from lithiation. The key assumption is to prescribe a homogeneous and normalized concentration field $c_{\mathrm{Li}} \in [0, 1]$ in the carbon fibres, in which the fibres are expanding anisotropically. Consequently, we can compute the accompanying stress response in the SBE. In order to carry out these computations, we employ computational homogenization methods to solve for an RVE problem; see works by Miehe et al. [47], Geers et al. [48], van Dijk [49] and Saeb et al. [50].

As the first step in establishing the model, let $\boldsymbol{u}$ denote the displacement field, additively decomposed into macroscopic (M) and microscopic (μ) parts so that $\boldsymbol{u} = \boldsymbol{u}^{\mathrm{M}} + \boldsymbol{u}^{\mu}$. The related deformation gradient can be expressed as

$$\boldsymbol{F} := \boldsymbol{I} + \boldsymbol{u} \otimes \boldsymbol{\nabla}_X = \bar{\boldsymbol{F}} + \boldsymbol{H}^{\mu}(\boldsymbol{u}^{\mu}), \tag{2.1}$$

where $\bar{\boldsymbol{F}} = \boldsymbol{I} + \boldsymbol{u}^{\mathrm{M}} \otimes \boldsymbol{\nabla}_X$ is referred to as the macroscopic deformation gradient and $\boldsymbol{H}^{\mu}(\boldsymbol{u}^{\mu}) = \boldsymbol{u}^{\mu} \otimes \boldsymbol{\nabla}_X$ is the microscopic displacement gradient. Furthermore, we introduce the volume averaging operator as

$$\langle \bullet \rangle_{\square} = \frac{1}{|\Omega_{\square}|} \int_{\Omega_{\square}} \bullet \, \mathrm{d}\Omega. \tag{2.2}$$

The negative electrode domain $\Omega_{\square}$, can be considered as macroscopically constrained or unconstrained, which is related to how much the external boundaries of the RVE are allowed to expand upon carbon fibre lithiation.

Introducing relevant constitutive relations for the carbon fibres and SBE, we can proceed to compute the (equilibrium) 1$^{\mathrm{st}}$ Piola-Kirchhoff stress $\boldsymbol{P} = \boldsymbol{P}(c_{\mathrm{Li}}, \boldsymbol{F})$

pertinent to the balance of linear momentum. A macroscopically *constrained* RVE domain is obtained by prescribing $\bar{\boldsymbol{F}} = \boldsymbol{I}$ such that the external boundaries of the RVE are fixed, and solving for the microscopic displacement field $\boldsymbol{u}^\mu$ given a lithium concentration field in the fibres. The weak form representation of the problem is expressed as[1]

$$\langle \boldsymbol{P}(c_{\mathrm{Li}}, \boldsymbol{I} + \boldsymbol{H}^\mu(\boldsymbol{u}^\mu)) : [\boldsymbol{H}^\mu(\delta\boldsymbol{u}^\mu) \otimes \boldsymbol{\nabla}_X] \rangle_\square = 0 \quad \forall \delta\boldsymbol{u}^\mu \in \mathbb{U}_\square. \tag{2.3}$$

As post-processing, we may evaluate the macroscopic 1st Piola-Kirchhoff stress as

$$\bar{\boldsymbol{P}}(c_{\mathrm{Li}}, \bar{\boldsymbol{F}})\Big|_{\bar{\boldsymbol{F}}=\boldsymbol{I}} = \langle \boldsymbol{P}(c_{\mathrm{Li}}, \boldsymbol{I} + \boldsymbol{H}^\mu(\boldsymbol{u}^\mu)) \rangle_\square. \tag{2.4}$$

In contrast, an *unconstrained* RVE domain is obtained when the negative electrode is macroscopically stress free. In other words, we seek a macroscopic deformation gradient, $\bar{\boldsymbol{F}}$, such that $\bar{\boldsymbol{P}} = \langle \boldsymbol{P} \rangle_\square = 0$. However, the problem of finding $\bar{\boldsymbol{F}}$ for known $\bar{\boldsymbol{P}}$ is ill-posed (contains infinitely many solutions) due to rigid-body rotations in the deformation gradient. To mitigate this issue, the macroscopic deformation gradient is multiplicatively decomposed into rotation $\bar{\boldsymbol{R}}$, and stretch $\bar{\boldsymbol{U}}$ parts

$$\bar{\boldsymbol{F}} = \bar{\boldsymbol{R}} \cdot \bar{\boldsymbol{U}}. \tag{2.5}$$

One can show that the implicit macroscopic stress relation is objective[2]

$$\bar{\boldsymbol{P}}(c_{\mathrm{Li}}, \bar{\boldsymbol{R}} \cdot \bar{\boldsymbol{U}}) = \bar{\boldsymbol{R}} \cdot \bar{\boldsymbol{P}}(c_{\mathrm{Li}}, \bar{\boldsymbol{U}}). \tag{2.6}$$

In a variational setting, we identify the conjugate stress to $\bar{\boldsymbol{U}}$ as

$$\langle \boldsymbol{P}(c_{\mathrm{Li}}, \boldsymbol{F}) : \delta\bar{\boldsymbol{F}} \rangle_\square = \left[\bar{\boldsymbol{R}}^T \cdot \bar{\boldsymbol{P}}\right] : \delta\bar{\boldsymbol{U}} = \bar{\boldsymbol{T}} : \delta\bar{\boldsymbol{U}}, \tag{2.7}$$

where $\bar{\boldsymbol{T}} = \left[\bar{\boldsymbol{R}}^T \cdot \bar{\boldsymbol{P}}\right]^{\mathrm{sym}}$ is the (symmetric) Biot stress.

Hence, assuming $\bar{\boldsymbol{R}} = \boldsymbol{I}$, the complete mixed form problem becomes to find $(\boldsymbol{u}^\mu, \bar{\boldsymbol{U}}) \in \mathbb{U}_\square \times \mathbb{R}^{3\times3,\mathrm{sym}}$ so that

$$\langle \boldsymbol{P}(c_{\mathrm{Li}}, \bar{\boldsymbol{U}} + \boldsymbol{H}^\mu(\boldsymbol{u}^\mu)) : \boldsymbol{H}^\mu(\delta\boldsymbol{u}^\mu) \rangle_\square = 0 \quad \forall \delta\boldsymbol{u}^\mu \in \mathbb{U}_\square, \tag{2.8a}$$

$$\langle \boldsymbol{P}(c_{\mathrm{Li}}, \bar{\boldsymbol{U}} + \boldsymbol{H}^\mu(\boldsymbol{u}^\mu)) \rangle_\square : \delta\bar{\boldsymbol{U}} = \bar{\boldsymbol{T}} : \delta\bar{\boldsymbol{U}} \quad \forall \delta\bar{\boldsymbol{U}} \in \mathbb{R}^{3\times3,\mathrm{sym}}, \tag{2.8b}$$

for a prescribed macroscopic Biot stress $\bar{\boldsymbol{T}}$, and a given concentration field in the fibres. In the present setting, the Biot stress can be prescribed to zero to represent an *unconstrained*, freely expanding, RVE where we solve for the macroscopic stretch components in $\bar{\boldsymbol{U}}$ as well as the microscopic displacement field $\boldsymbol{u}^\mu$.

[1] We note that appropriate boundary conditions must be chosen in $\mathbb{U}_\square$ such that $\langle \boldsymbol{u}^\mu \rangle = 0$.

[2] This relation holds under the condition that the microscale material models are invariant to macroscopic rotations.

A detailed description of the constitutive model for the carbon fibres is presented in Section 2.2. To accurately capture the internal stress distribution arising from fibre lithiation, a poro-viscoelastic formulation was adopted for the SBE in **Paper B**, providing a representative description of the coupled solid–fluid interactions within the composite microstructure. The constitutive model of the SBE, as presented in Section 2.3, was calibrated using compressive mechanical experiments together with measurements of fluid mass loss, allowing characterization of both the mechanical response and fluid-transport properties of the matrix material.

Furthermore, an additional factor governing the stress distribution within the matrix is the microstructural morphology and the spatial arrangement of the carbon fibres. In **Paper C**, SEM-image informed microscale RVEs were generated to accurately reproduce realistic fibre volume fractions and stochastic arrangements. These RVEs were integrated with the calibrated constitutive model for the SBE from **Paper B** and the constitutive model for carbon fibres developed in **Paper A** to simulate the internal stress states during lithiation.

2.2 Carbon fibres

For the fibre domain Ω^{f} in **Paper A** and **Paper C**, we adopt a hyperelastic model accounting for "free" deformation caused by lithium insertion in the lattice. We then adopt, in standard fashion, the multiplicative split of the deformation gradient so that

$$\boldsymbol{F} = \boldsymbol{F}^{\mathrm{e}} \cdot \boldsymbol{F}^{\mathrm{ch}}(c_{\mathrm{Li}}) \tag{2.9}$$

where $\boldsymbol{F}^{\mathrm{e}}$ is the elastic deformation gradient, whereas $\boldsymbol{F}^{\mathrm{ch}}(c_{\mathrm{Li}})$ is the chemical deformation gradient due to insertion and is defined by the insertion tensor $\boldsymbol{\alpha}^{\mathrm{ch}}$,

$$\boldsymbol{F}^{\mathrm{ch}}(c_{\mathrm{Li}}) = \boldsymbol{I} + \boldsymbol{\alpha}^{\mathrm{ch}} c_{\mathrm{Li}}, \quad \boldsymbol{\alpha}^{\mathrm{ch}} = \alpha_{\mathrm{L}}^{\mathrm{ch}} \boldsymbol{e}_1 \otimes \boldsymbol{e}_1 + \alpha_{\mathrm{T}}^{\mathrm{ch}} \left[\boldsymbol{e}_2 \otimes \boldsymbol{e}_2 + \boldsymbol{e}_3 \otimes \boldsymbol{e}_3\right], \tag{2.10}$$

that reflects transverse isotropy with basis $\boldsymbol{e}_1$ associated with the longitudinal direction and $\boldsymbol{e}_2$, $\boldsymbol{e}_3$ in the transversely isotropic plane. Using (2.9) and (2.10), we may compute the corresponding elastic Green-Lagrange strain

$$\boldsymbol{E}^{\mathrm{e}} := [\boldsymbol{F}^{\mathrm{ch}}]^{-\mathrm{T}} \cdot \left[\boldsymbol{E} - \boldsymbol{E}^{\mathrm{ch}}\right] \cdot [\boldsymbol{F}^{\mathrm{ch}}]^{-1} \tag{2.11}$$

where

$$\boldsymbol{E} = \frac{1}{2}[\boldsymbol{F}^{\mathrm{T}} \cdot \boldsymbol{F} - \boldsymbol{I}], \quad \boldsymbol{E}^{\mathrm{ch}}(c_{\mathrm{Li}}) = \frac{1}{2}[[\boldsymbol{F}^{\mathrm{ch}}(c_{\mathrm{Li}})]^{\mathrm{T}} \cdot \boldsymbol{F}^{\mathrm{ch}}(c_{\mathrm{Li}}) - \boldsymbol{I}]. \tag{2.12}$$

For the particular choice of $\boldsymbol{\alpha}^{\mathrm{ch}}$ in (2.10), we obtain

$$\begin{aligned} \boldsymbol{E}^{\mathrm{ch}}(c_{\mathrm{Li}}) = &\left[2\alpha_{\mathrm{L}}^{\mathrm{ch}} c_{\mathrm{Li}} + [\alpha_{\mathrm{L}}^{\mathrm{ch}}]^2 c_{\mathrm{Li}}^2\right] \boldsymbol{e}_1 \otimes \boldsymbol{e}_1 \\ &+ \left[2\alpha_{\mathrm{T}}^{\mathrm{ch}} c_{\mathrm{Li}} + [\alpha_{\mathrm{T}}^{\mathrm{ch}}]^2 c_{\mathrm{Li}}^2\right] \left[\boldsymbol{e}_2 \otimes \boldsymbol{e}_2 + \boldsymbol{e}_3 \otimes \boldsymbol{e}_3\right]. \end{aligned} \tag{2.13}$$

Next, we introduce the free energy density ψ in the material format

$$\psi = \psi(\boldsymbol{E}^{\mathrm{e}}(\boldsymbol{E}, c_{\mathrm{Li}})) = \frac{1}{2}\boldsymbol{E}^{\mathrm{e}}(\boldsymbol{E}, c_{\mathrm{Li}}) : \mathsf{E}_{\mathrm{f}}(c_{\mathrm{Li}}) : \boldsymbol{E}^{\mathrm{e}}(\boldsymbol{E}, c_{\mathrm{Li}}). \tag{2.14}$$

As to the introduced variables and constitutive parameters, $\mathsf{E}_{\mathrm{f}}(c_{\mathrm{Li}})$ is the small strain Hooke tensor representing transverse elastic isotropy[3]. We note that $\mathsf{E}_{\mathrm{f}}(c_{\mathrm{Li}})$ corresponds exactly to the linearization of the stress-strain response at an expanded, stress free state, due to lithiation. Thereby its coefficients are directly determined from the measurements in [23]. The particular choice of ψ in (2.14) represents the St-Venant model of hyper-elasticity w.r.t the intermediate configuration. The 2$^{\mathrm{nd}}$ Piola-Kirchhoff stress $\boldsymbol{S}$ can then be derived as

$$\boldsymbol{S} = \frac{\partial \psi}{\partial \boldsymbol{E}} = [\boldsymbol{F}^{\mathrm{ch}}]^{-1} \cdot \boldsymbol{S}^{\mathrm{e}} \cdot [\boldsymbol{F}^{\mathrm{ch}}]^{-\mathrm{T}} \quad \text{with } \boldsymbol{S}^{\mathrm{e}} := \mathsf{E}_{\mathrm{f}}(c_{\mathrm{Li}}) : \boldsymbol{E}^{\mathrm{e}}. \tag{2.15}$$

Clearly, $\boldsymbol{S}^{\mathrm{e}}$ is the 2$^{\mathrm{nd}}$ Piola-Kirchhoff stress on the intermediate configuration that is obtained from push-forward of $\boldsymbol{S}$ as follows

$$\boldsymbol{S}^{\mathrm{e}} := \boldsymbol{F}^{\mathrm{ch}} \cdot \boldsymbol{S} \cdot [\boldsymbol{F}^{\mathrm{ch}}]^{\mathrm{T}}. \tag{2.16}$$

Combining (2.15) with (2.11), we arrive at the constitutive relation

$$\boldsymbol{S} := \mathsf{L}(c_{\mathrm{Li}}) : [\boldsymbol{E} - \boldsymbol{E}^{\mathrm{ch}}(c_{\mathrm{Li}})] \tag{2.17}$$

where the Li-concentration dependent elastic stiffness L is given as

$$\mathsf{L}(c_{\mathrm{Li}}) := \left[[\boldsymbol{F}^{\mathrm{ch}}(c_{\mathrm{Li}})]^{-1} \bar{\otimes} [\boldsymbol{F}^{\mathrm{ch}}(c_{\mathrm{Li}})]^{-1}\right] : \mathsf{E}_{\mathrm{f}}(c_{\mathrm{Li}}) : \left[[\boldsymbol{F}^{\mathrm{ch}}(c_{\mathrm{Li}})]^{-\mathrm{T}} \bar{\otimes} [\boldsymbol{F}^{\mathrm{ch}}(c_{\mathrm{Li}})]^{-\mathrm{T}}\right]. \tag{2.18}$$

2.3 Structural Battery Electrolyte (SBE)

The structural battery electrolyte is represented as a continuum porous medium. Based on the principle of effective stress, the total 2$^{\mathrm{nd}}$ Piola-Kirchhoff stress $\boldsymbol{S}$ is decomposed into a mechanical contribution from the solid skeleton, $\boldsymbol{S}'$, and a contribution from the pore pressure p. In accordance with Terzaghi's theory [51], we assume that the solid phase is intrinsically incompressible so that the density of the solid phase is constant $\rho^{\mathrm{s}} = \rho_0^{\mathrm{s}}$. Under this assumption, the total stress is expressed as

$$\boldsymbol{S} = \boldsymbol{S}' - Jp\boldsymbol{C}^{-1} \tag{2.19}$$

[3] E depend on the lithium concentration c_{Li} in the fibres; specifically, the longitudinal and transverse moduli $E_{\mathrm{L}} = E_{\mathrm{L}}(c_{\mathrm{Li}})$, $E_{\mathrm{T}} = E_{\mathrm{T}}(c_{\mathrm{Li}})$.

where $J = \det(\boldsymbol{F})$ is the determinant of the deformation gradient and $\boldsymbol{C}$ is the Cauchy-Green deformation tensor.

For the electrolyte solid skeleton we adopt a visco-hyperelastic model that represents a finite deformation extension of the classical Zener model (sometimes denoted Three-Parameter Model), see Figure 3 in **Paper B**. In order to represent the viscous response in a realistic fashion, we consider the "non-equilibrium chain" and introduce the multiplicative split

$$\boldsymbol{F} = \boldsymbol{F}^{\mathrm{e}} \cdot \boldsymbol{F}^{\mathrm{v}} \tag{2.20}$$

where, once again, $\boldsymbol{F}^{\mathrm{e}}$ represents elastic deformation, whereas $\boldsymbol{F}^{\mathrm{v}}$ is the viscous deformation, cf. Reese and Govindjee [52]. In this case we adopt the formulation of a Neo-Hooke model. Similarly to the steps of the derivation for the fibre, whereby $\boldsymbol{F}^{\mathrm{v}}$ now plays a role that is similar to that of the insertion deformation $\boldsymbol{F}^{\mathrm{ch}}$, we conclude that the relevant elastic deformation $\boldsymbol{C}^{\mathrm{e}}$ for the "non-equilibrium chain" can be expressed as

$$\boldsymbol{C}^{\mathrm{e}} := [\boldsymbol{F}^{\mathrm{v}}]^{-\mathrm{T}} \cdot \boldsymbol{C} \cdot [\boldsymbol{F}^{\mathrm{v}}]^{-1} \quad \text{with } \boldsymbol{C} := \boldsymbol{F}^{\mathrm{T}} \cdot \boldsymbol{F} \tag{2.21}$$

Next, we introduce the free energy density ψ in the material format, which is split additively into equilibrium and non-equilibrium parts, associated with the static spring and dashpot-spring branches as

$$\psi = \psi^{\mathrm{EQ}} + \psi^{\mathrm{NEQ}}. \tag{2.22}$$

The response of the equilibrium spring is expressed in terms of the total deformation $\psi^{\mathrm{EQ}} = \psi^{\mathrm{EQ}}(\boldsymbol{C})$, whereas the non-equilibrium branch free energy is expressed in terms of the elastic deformation $\psi^{\mathrm{NEQ}} = \psi^{\mathrm{NEQ}}(\boldsymbol{C}^{\mathrm{e}})$. We then derive (in standard fashion) the effective 2$^{\mathrm{nd}}$ Piola-Kirchhoff stress

$$\boldsymbol{S}' = 2\frac{\partial \psi}{\partial \boldsymbol{C}} = 2\left[\frac{\partial \psi^{\mathrm{EQ}}}{\partial \boldsymbol{C}} + \frac{\partial \psi^{\mathrm{NEQ}}}{\partial \boldsymbol{C}^{\mathrm{e}}} : \frac{\partial \boldsymbol{C}^{\mathrm{e}}}{\partial \boldsymbol{C}}\right]. \tag{2.23}$$

It remains to define the evolution rule for $\boldsymbol{F}^{\mathrm{v}}$. We propose the following Norton-type model

$$\boldsymbol{l}^{\mathrm{v}} := \dot{\boldsymbol{F}}^{\mathrm{v}} \cdot [\boldsymbol{F}^{\mathrm{v}}]^{-1} = \frac{1}{t^*}\left[\frac{\bar{M}}{\sigma_y}\right]^{n_{\mathrm{c}}} \frac{3\boldsymbol{M}_{\mathrm{dev}}}{2\bar{M}} \tag{2.24}$$

where we introduce the Mandel stress $\boldsymbol{M} := \boldsymbol{C}^{\mathrm{e}} \cdot 2\frac{\partial \psi^{\mathrm{NEQ}}}{\partial \boldsymbol{C}^{\mathrm{e}}}$ with the split into deviatoric and volumetric parts

$$\boldsymbol{M} = \boldsymbol{M}_{\mathrm{dev}} + \frac{1}{3}\mathrm{tr}(\boldsymbol{M})\boldsymbol{I}, \quad \bar{M} := \sqrt{\frac{3}{2}}|\boldsymbol{M}_{\mathrm{dev}}|. \tag{2.25}$$

We note that the presented constitutive response is applicable for the drained solid skeleton with an incompressible solid phase. In contrast, compressibility is introduced in the fluid phase. In the present setting, the current porosity can be derived as

$$\phi(J) = 1 - \frac{1}{J}[1 - \phi_0], \tag{2.26}$$

where ϕ_0 is the initial (undeformed) porosity. The evolution of fluid density is expressed as

$$\rho^{\mathrm{F}}(p) = \rho_0^{\mathrm{F}} \left[1 + \frac{p}{\kappa^{\mathrm{F}}}\right], \tag{2.27}$$

where κ^{F} denotes the intrinsic bulk modulus of the fluid. The liquid electrolyte transport is represented with a Darcy type law in the reference configuration, expressed as

$$\phi \boldsymbol{W} = -\boldsymbol{K} \cdot \boldsymbol{\nabla}_{\mathrm{X}} p, \tag{2.28}$$

where $\boldsymbol{K}$ is the permeability tensor in the reference configuration. At this stage, we assume that the permeability is macroscopically isotropic, such that $\boldsymbol{K} = K\boldsymbol{I}$.

2.4 Micromechanical analysis of the negative electrode

Upon combining the developed constitutive models in **Papers A** and **B** with a SEM-informed RVE from **Paper C**, and allowing the fibres to expand during lithiation, a complex internal stress state is obtained, as depicted in Figure 2.2. By solving the microscale boundary value problem using these constitutive relations, several observations regarding the mechanical performance of the structural negative electrode can be made:

i The use of realistic fibre arrangements highlights significant stress concentrations in the SBE matrix that are absent in idealized periodic fibre arrangements. In regions where fibres are closely packed due to manufacturing induced randomness, the localized compressive stresses are significantly higher.

ii The constitutive model for the SBE, which accounts for both viscous relaxation and Darcy-type fluid transport, introduces a rate-dependency to the internal stress state. During rapid lithiation, the restricted fluid mobility within the SBE leads to a transient stiffening effect. This indicates that internal stress peaks are not only a function of the state of charge but are also sensitive to the lithium insertion rate.

iii A notable result from the unconstrained RVE simulations is that the macroscopic longitudinal stretch, $\bar{U}_{11}$, is almost entirely governed by the fibre insertion tensor, effectively reaching the free expansion limit α_{L}.

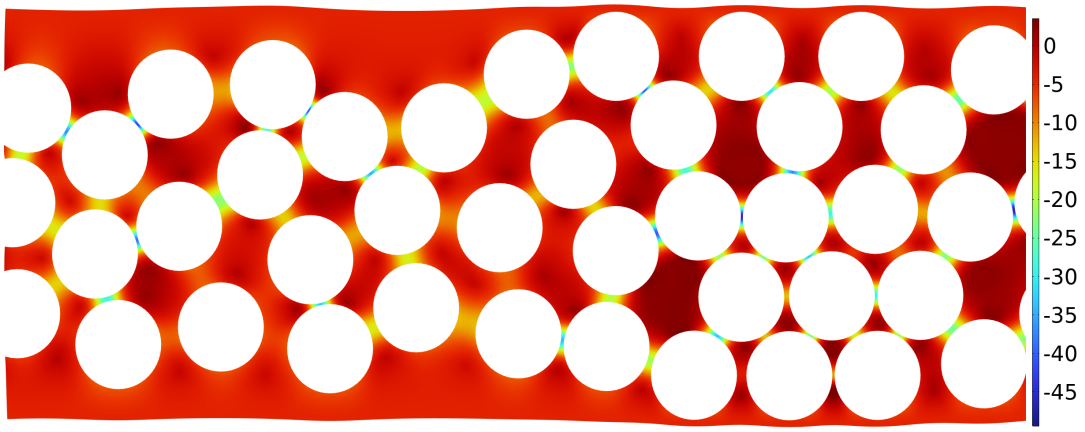

Figure 2.2: Minimum effective principal stress field in the SBE matrix at a state of full charge ($c_{\mathrm{Li}} = 1$), shown in MPa. The simulation accounts for the anisotropic expansion of the carbon fibres and the poro-viscous response of the matrix.

3

Electro-chemo-mechanical modelling of the structural battery full cell

3.1 The structural battery full cell

In this chapter, focus is placed on the formulation of the electro-chemo-mechanical processes governing the multiphysics response of a structural battery full cell. While the microscale electrode analysis in the preceding chapter utilized a finite-strain framework, the full cell formulation adopted here considers small deformations. Further emphasis is placed on the thermodynamic coupling between the chemical and mechanical fields; specifically, we address how the application of mechanical loading produces a change in the electric potential. By extending the Helmholtz free energy functionals, we derive the corresponding constitutive responses pertaining to the governing differential equations.

In **Paper D**, we present a fully coupled electro-chemo-mechanical model for a structural battery composite full cell. The material parameters associated with these constitutive relations are calibrated against experimental galvanostatic charge-discharge curves. Building upon this framework, **Paper E** introduces a specific focus on the experimental findings and numerical modelling of the electro-chemo-mechanical coupling. In particular, we calibrate the proposed model to capture the electric potential variations induced by applied mechanical load, providing a basis for understanding the multifunctional processes in structural batteries.

3.2 Balance equations

To model the coupled electro-chemo-mechanical processes in a structural lithium-ion battery, depicted in Figure 3.1, we consider the following set of balance equations representing momentum, charge, and mass

$$-\boldsymbol{\sigma} \cdot \boldsymbol{\nabla} = 0 \quad \text{in} \quad \Omega, \tag{3.1a}$$

$$F[c_{\mathrm{Li}} - c_{\mathrm{X}}] - \boldsymbol{d} \cdot \boldsymbol{\nabla} = 0 \quad \text{in} \quad \Omega^{\mathrm{SBE}} \cup \Omega^{\mathrm{SEP}}, \tag{3.1b}$$

$$\partial_t c_\alpha + \boldsymbol{j}_\alpha \cdot \boldsymbol{\nabla} = 0 \quad \text{in} \quad \Omega^{\mathrm{SBE}} \cup \Omega^{\mathrm{SEP}}, \quad \alpha = \mathrm{Li}, \mathrm{X}, \tag{3.1c}$$

$$\partial_t c_{\mathrm{Li}} + \boldsymbol{j}_{\mathrm{Li}} \cdot \boldsymbol{\nabla} = 0 \quad \text{in} \quad \Omega^{\mathrm{f}} \cup \Omega^{\mathrm{p}}. \tag{3.1d}$$

In these expressions, $\boldsymbol{\sigma}$ represents the stress tensor in the balance of linear momentum in Eq. (3.1a). Eq. (3.1b) describes the balance of charge, where $\boldsymbol{d}$ is the electric displacement vector and F is Faraday's constant; here, the difference between the lithium-ion c_{Li} and anion c_{X} concentrations represents the local ionic charge imbalance. The mass conservation for the electrolyte species and the active electrode materials are given by Eqs. (3.1c) and (3.1d), respectively, where c_α denotes the molar concentration of species α and $\boldsymbol{j}_\alpha$ represents its corresponding flux. The charge balance is not explicitly solved in the active electrode domains Ω^{f} and Ω^{p}; this effectively assumes that the electronic conductivity in these regions is sufficiently high to motivate the assumption that the electric potential is uniform in these domains.

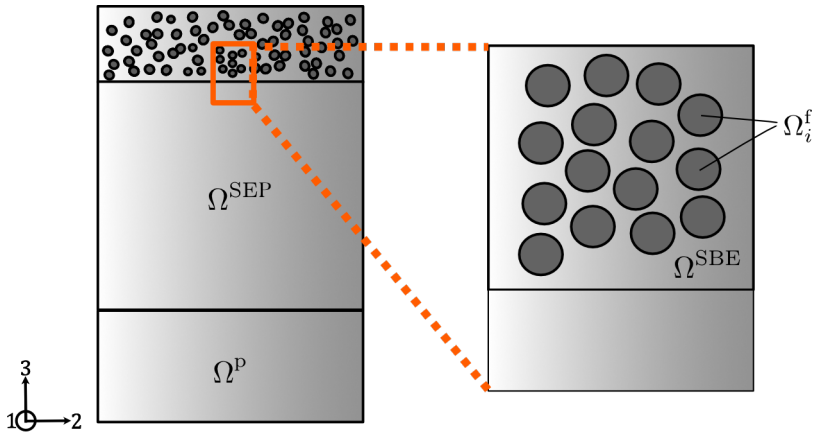

Figure 3.1: Illustration of the structural battery full cell computational domain, consisting of the positive electrode domain Ω^{p}, the carbon fibre domain Ω^{f}, the separator domain Ω^{SEP} and SBE domain Ω^{SBE}.

3.3 Constitutive equations

3.3.1 Electrodes

As previously mentioned, the active electrodes are composed of materials that undergo significant concentration dependent changes in their mechanical properties and volume upon lithiation. The Helmholtz free energy ψ_β for carbon fibres in the negative electrode and positive electrode phase $\beta \in \{\mathrm{f}, \mathrm{p}\}$ is decomposed into elastic and chemical contributions as

$$\psi_\beta(\boldsymbol{\epsilon}, c_{\mathrm{Li}}) = \frac{1}{2}\left[\boldsymbol{\epsilon} - \boldsymbol{\epsilon}^{\mathrm{ch}}\right] : \mathbf{E}_\beta(c_{\mathrm{Li}}) : \left[\boldsymbol{\epsilon} - \boldsymbol{\epsilon}^{\mathrm{ch}}\right] + \bar{\psi}_\beta(c_{\mathrm{Li}}, \tilde{c}_\beta - c_{\mathrm{Li}}). \tag{3.2a}$$

The chemical expansion strain is defined as

$$\boldsymbol{\epsilon}^{\mathrm{ch}} = \boldsymbol{\alpha}_\beta \frac{c_{\mathrm{Li}} - c^{\mathrm{ref}}_{\mathrm{Li},\beta}}{\tilde{c}_\beta} \tag{3.2b}$$

where $c^{\mathrm{ref}}_{\mathrm{Li},\beta}$ is an initial reference value of the lithium concentration, $\tilde{c}_\beta$ is the maximum concentration and $\boldsymbol{\epsilon}$ denotes the (small) strain tensor. For the carbon fibres, the chemical expansion $\boldsymbol{\alpha}_{\mathrm{f}}$ is transversely isotropic, including longitudinal and transverse expansion coefficients. Conversely, for the positive electrode, an isotropic expansion behaviour is assumed so that $\boldsymbol{\alpha}_{\mathrm{p}} = \alpha_{\mathrm{p}}\boldsymbol{I}$. An additional property of the electrodes is the concentration of vacant sites denoted $c_{v,\mathrm{Li}}$. The concentration of vacant sites together with the lithium concentration constitutes the maximum concentration of the electrode. In this work we assume that the maximum concentration of the electrodes are constant, which implies a system of zero losses such that $\tilde{c}_\beta = c_{\mathrm{Li}} + c_{v,\mathrm{Li}}$ for constant $\tilde{c}_\beta$, cf. Bucci et al. [45]. Hence, we express the chemical contribution $\bar{\psi}_\beta$ as

$$\bar{\psi}_\beta(c_{\mathrm{Li}}, c_{\mathrm{v}}) = c_{\mathrm{Li}}\mu^0_{\mathrm{Li},\beta} + c_{\mathrm{v}}\mu^0_{\mathrm{v},\beta} + RT\left[c_{\mathrm{Li}}\ln(c_{\mathrm{Li}}) + c_{\mathrm{v}}\ln(c_{\mathrm{v}})\right] + \Lambda_\beta(c_{\mathrm{Li}}, c_{\mathrm{v}}). \tag{3.2c}$$

In this expression, $\mu^0_{\mathrm{Li},\beta}$ and $\mu^0_{\mathrm{v},\beta}$ are the reference chemical potential for lithium and vacant sites, R is the ideal gas constant and T the temperature. The fourth-order elastic stiffness tensor $\mathbf{E}_\beta$ characterizes the mechanical response of the electrode phases. For the carbon fibres, $\mathbf{E}_{\mathrm{f}}(c_{\mathrm{Li}})$ is defined as concentration-dependent to capture the effects on the carbon fibres moduli during lithiation. The stiffness of the positive electrode $\mathbf{E}_{\mathrm{p}}$ is assumed to be constant. The term Λ_β in (3.2c) accounts for the deviation from ideal conditions due to the interaction between the lithium concentration and vacant site, characterized by a material-specific solubility parameter k_β [53].

The constitutive relations for the active electrodes are derived by taking the partial derivatives of the Helmholtz free energy with respect to the strain and

concentration, respectively. For the carbon fibres in the negative electrode, the stress tensor $\boldsymbol{\sigma}$ and the chemical potential μ_{Li} are obtained as

$$\boldsymbol{\sigma}(\boldsymbol{\epsilon}, c_{\mathrm{Li}}) = \frac{\partial \psi_{\mathrm{f}}}{\partial \boldsymbol{\epsilon}} = \mathbf{E}_{\mathrm{f}}(c_{\mathrm{Li}}) : \left[\boldsymbol{\epsilon} - \boldsymbol{\alpha}_{\mathrm{f}} \frac{c_{\mathrm{Li}} - c_{\mathrm{Li,f}}^{\mathrm{ref}}}{\tilde{c}_{\mathrm{f}}} \right], \tag{3.3a}$$

$$\begin{aligned} \mu_{\mathrm{Li}}(\boldsymbol{\epsilon}, c_{\mathrm{Li}}) = \frac{\partial \psi_{\mathrm{f}}}{\partial c_{\mathrm{Li}}} = &- \frac{1}{\tilde{c}_{\mathrm{f}}} \boldsymbol{\alpha}_{\mathrm{f}} : \boldsymbol{\sigma} + \mu_{\mathrm{f}}^{0} + RT \left[\ln \left(\frac{c_{\mathrm{Li}}}{\tilde{c}_{\mathrm{f}} - c_{\mathrm{Li}}} \right) + k_{\mathrm{f}} \left(1 - \frac{c_{\mathrm{Li}}}{\tilde{c}_{\mathrm{f}}} \right) \right] + \\ &\frac{1}{2} \boldsymbol{\sigma} : \left[\mathbf{E}_{\mathrm{f}}(c_{\mathrm{Li}}) \right]^{-1} : \frac{\partial \mathbf{E}_{\mathrm{f}}(c_{\mathrm{Li}})}{\partial c_{\mathrm{Li}}} : \left[\mathbf{E}_{\mathrm{f}}(c_{\mathrm{Li}}) \right]^{-1} : \boldsymbol{\sigma}. \end{aligned} \tag{3.3b}$$

In Eq. (3.3b), the first term represents the stress-coupling governed by the chemical expansion $\boldsymbol{\alpha}_{\mathrm{f}}$, while the last term accounts for the energy change associated with the concentration-dependent elastic moduli. Finally, the mass flux of neutral lithium within the carbon fibres is governed by the gradient of the chemical potential, scaled by the mobility coefficient $M_{\mathrm{Li,f}}$, as

$$\boldsymbol{j}_{\mathrm{Li}} = -M_{\mathrm{Li,f}}(c_{\mathrm{Li}}) \boldsymbol{\nabla} \mu_{\mathrm{Li}}, \tag{3.4}$$

where $M_{\mathrm{Li,f}}$ is assumed to be isotropic in the transverse plane of the fibres.

Similarly, the constitutive relations for the positive electrode phase are obtained from the free energy ψ_{p}. Given the assumption of constant elastic properties and isotropic chemical expansion for this phase, the stress and chemical potential simplify to

$$\boldsymbol{\sigma}(\boldsymbol{\epsilon}, c_{\mathrm{Li}}) = \frac{\partial \psi_{\mathrm{p}}}{\partial \boldsymbol{\epsilon}} = \mathbf{E}_{\mathrm{p}} : \left[\boldsymbol{\epsilon} - \alpha_{\mathrm{p}} \frac{c_{\mathrm{Li}} - c_{\mathrm{Li,p}}^{\mathrm{ref}}}{\tilde{c}_{\mathrm{p}}} \boldsymbol{I} \right], \tag{3.5a}$$

$$\mu_{\mathrm{Li}}(\boldsymbol{\epsilon}, c_{\mathrm{Li}}) = \frac{\partial \psi_{\mathrm{p}}}{\partial c_{\mathrm{Li}}} = -\frac{\alpha_{\mathrm{p}}}{\tilde{c}_{\mathrm{p}}} \mathrm{tr}(\boldsymbol{\sigma}) + \mu_{\mathrm{p}}^{0} + RT \left[\ln \left(\frac{c_{\mathrm{Li}}}{\tilde{c}_{\mathrm{p}} - c_{\mathrm{Li}}} \right) + k_{\mathrm{p}} \left(1 - \frac{c_{\mathrm{Li}}}{\tilde{c}_{\mathrm{p}}} \right) \right]. \tag{3.5b}$$

In Eq. (3.5b), the coupling term solely depends on the trace of the stress tensor. The transport of lithium within the positive electrode particles is likewise driven by the chemical potential gradient

$$\boldsymbol{j}_{\mathrm{Li}} = -M_{\mathrm{Li,p}}(c_{\mathrm{Li}}) \boldsymbol{\nabla} \mu_{\mathrm{Li}}, \tag{3.6}$$

where $M_{\mathrm{Li,p}}$ denotes the isotropic mobility coefficient for the positive electrode.

3.3.2 SBE and separator domains

In the electrolyte and separator domains, the Helmholtz free energy ψ accounts for the elastic energy of the porous skeleton, the chemical energy of the electrolyte,

and the electrostatic energy as

$$\psi_\omega(\boldsymbol{\epsilon}, c_\alpha, \varphi) = \frac{1}{2}\boldsymbol{\epsilon} : \mathbf{E}_\omega : \boldsymbol{\epsilon} + \sum_\alpha c_\alpha \left[\mu_\alpha^0 + RT \ln\left(\frac{c_\alpha}{c_{\text{ref}}}\right) - RT\right] - \frac{1}{2}\varepsilon(\boldsymbol{\nabla}\varphi)^2, \tag{3.7}$$

for species $\alpha \in \{\text{Li, X}\}$ and domain $\omega \in \{\text{SBE, SEP}\}$. Here, ε denotes the permittivity and c_{ref} is the salt concentration in the electrolyte. The effective stiffness tensor $\mathbf{E}_\omega$ is defined according to the specific region; while $\mathbf{E}_{\text{SBE}}$ characterizes the structural electrolyte, the separator stiffness $\mathbf{E}_{\text{SEP}}$ as well as mobility coefficients $\eta_{\text{Li,SEP}}$ and $\eta_{\text{X,SEP}}$ are determined via a mixture-relation that incorporates the contribution of the glass fibre reinforcement and SBE materials. The derived constitutive relations for the stress, chemical potentials, and electric displacement becomes

$$\boldsymbol{\sigma} = \frac{\partial \psi_\omega}{\partial \boldsymbol{\epsilon}} = \mathbf{E}_\omega : \boldsymbol{\epsilon}, \tag{3.8a}$$

$$\mu_\alpha = \frac{\partial \psi_\omega}{\partial c_\alpha} = \mu_\alpha^0 + RT \ln\left(\frac{c_\alpha}{c_{\text{ref}}}\right), \tag{3.8b}$$

$$\boldsymbol{d} = \frac{\partial \psi_\omega}{\partial \boldsymbol{\nabla}\varphi} = -\varepsilon \boldsymbol{\nabla}\varphi. \tag{3.8c}$$

The ionic transport within the liquid phase of these domains is driven by the electrochemical potential gradients, resulting in the mass fluxes

$$\boldsymbol{j}_{\text{Li}} = -\eta_{\text{Li},\omega} c_{\text{Li}} \left[\boldsymbol{\nabla}\mu_{\text{Li}} + F\boldsymbol{\nabla}\varphi\right], \tag{3.9a}$$

$$\boldsymbol{j}_{\text{X}} = -\eta_{\text{X},\omega} c_{\text{X}} \left[\boldsymbol{\nabla}\mu_{\text{X}} - F\boldsymbol{\nabla}\varphi\right], \tag{3.9b}$$

where $\eta_{\alpha,\omega}$ denotes the domain-specific ionic mobility coefficient for either lithium cations or the corresponding anion. The coupling of the chemical and electrical fields is explicitly captured in the flux relations, where the valence of the species determines the direction of migration. Specifically, the lithium cations (Li^+) are positively charged with a valance number of +1, while the corresponding anions (X^-) are negatively charged with a valance number of -1. As a consequence, the migration parts of $\boldsymbol{j}_{\text{Li}}$ and $\boldsymbol{j}_{\text{X}}$ have opposite directions

3.3.3 Interface conditions

The interface between the electrodes and the electrolyte, denoted as Γ, is characterized by the reaction of lithium species between a neutral atomic state within the electrode and an ionic state in the electrolyte, see Figure 6 in **Paper D**. Across these boundaries, the mass flux $j_n = \boldsymbol{j}_{\text{Li}} \cdot \boldsymbol{n}$ is assumed to be continuous, where $\boldsymbol{n}$ is the unit normal vector pointing outward from the electrode domain. Conversely,

the chemical and electric potentials exhibit jumps across the interface, denoted as $[\![\mu_{\mathrm{Li}}]\!]$ and $[\![\varphi]\!]$, respectively. The kinetics of the interfacial mass flux are governed by the classical Butler-Volmer equation, relating the reaction rate to the electro-chemical overpotential η as

$$j_n = \frac{i_0(c_{\mathrm{Li}})}{F}\left[\exp\left(\frac{\eta}{2RT}\right) - \exp\left(\frac{-\eta}{2RT}\right)\right], \tag{3.10a}$$

$$\eta = F[\![\varphi]\!] + [\![\mu_{\mathrm{Li}}]\!]. \tag{3.10b}$$

The exchange current density $i_0(c_{\mathrm{Li}})$ represents the rate of the charge-transfer reaction at the respective interface. In this formulation, i_0 is defined as a concentration-dependent parameter to capture the varying reaction kinetics as a function of the local lithium concentration in the electrode host. To ensure mass conservation at the interface, it is assumed that no concentration accumulation occurs, such that the normal flux is continuous over the boundary, i.e., $[\![\boldsymbol{j}_{\mathrm{Li}}]\!] \cdot \boldsymbol{n} = 0$. The corresponding interfacial electric current density i_n is determined via Faraday's law of electrolysis as

$$i_n = F j_n. \tag{3.11}$$

Furthermore, for the case where interface charge accumulation is neglected, it is assumed that the normal component of the electric displacement d_n is coupled to the mass flux according to

$$d_n = -\frac{\varepsilon}{\kappa} F j_n, \tag{3.12}$$

where ε and κ represent the effective electric permittivity and ionic conductivity of the homogenous positive electrode or carbon fibres, respectively.

3.4 Multifunctional characterization of the structural battery full cell

The numerical framework developed in **Paper D** and **Paper E** was utilized to investigate the multifunctional performance of the structural battery composite. The proposed fully coupled model incorporates a significant number of material parameters, spanning mechanical, chemical, and electrical domains. By utilizing experimental measurements to fix well-characterized parameters, such as elastic moduli, mobility coefficient and the exchange current density in the fibres, the remaining parameters were systematically calibrated against experiments. In **Paper D**, this calibration was performed against experimental galvanostatic discharge data, demonstrating that

i The model accurately captures the rate-dependent charge-rest-discharge profiles of the structural battery full cell. By incorporating the concentration-dependent mobility and Butler-Volmer kinetics, the voltage drop at higher C-rates is well predicted, as shown in Figure 3.2a.

ii As the result of a sensitivity study, it was concluded that the ionic conductivity of the SBE is the primary limiting factor for high-rate performance, rather than the solid-state diffusion within the carbon fibres.

Paper E is focused on the coupling between mechanical loading and electrochemical potential. This is a defining feature of multifunctional structural batteries. Key observations include the following

iii Both experimental measurements and numerical simulations show that applying a mechanical load to the full cell, induces a measurable change in the open-circuit potential (OCP). Moreover, we are able to calibrate parameters to fit the experimental data of mechanical loading induced OCP variation well, as shown in Figure 3.2b.

iv The simulations confirm that this potential shift is driven by the carbon fibres in the negative electrode, primarily through the term $-\frac{1}{\tilde{c}_\mathrm{f}}\boldsymbol{\alpha}_\mathrm{f} : \boldsymbol{\sigma}$ in Eq. (3.3b). When the carbon fibres are subjected to tensile or compressive stress, the chemical potential of the intercalated lithium is altered, forcing a redistribution of charge and a shift in the electric potential φ.

v The results demonstrate that the structural battery full cell can act as a sensor, where the change in electric potential can be associated with the mechanical strain state of the composite.

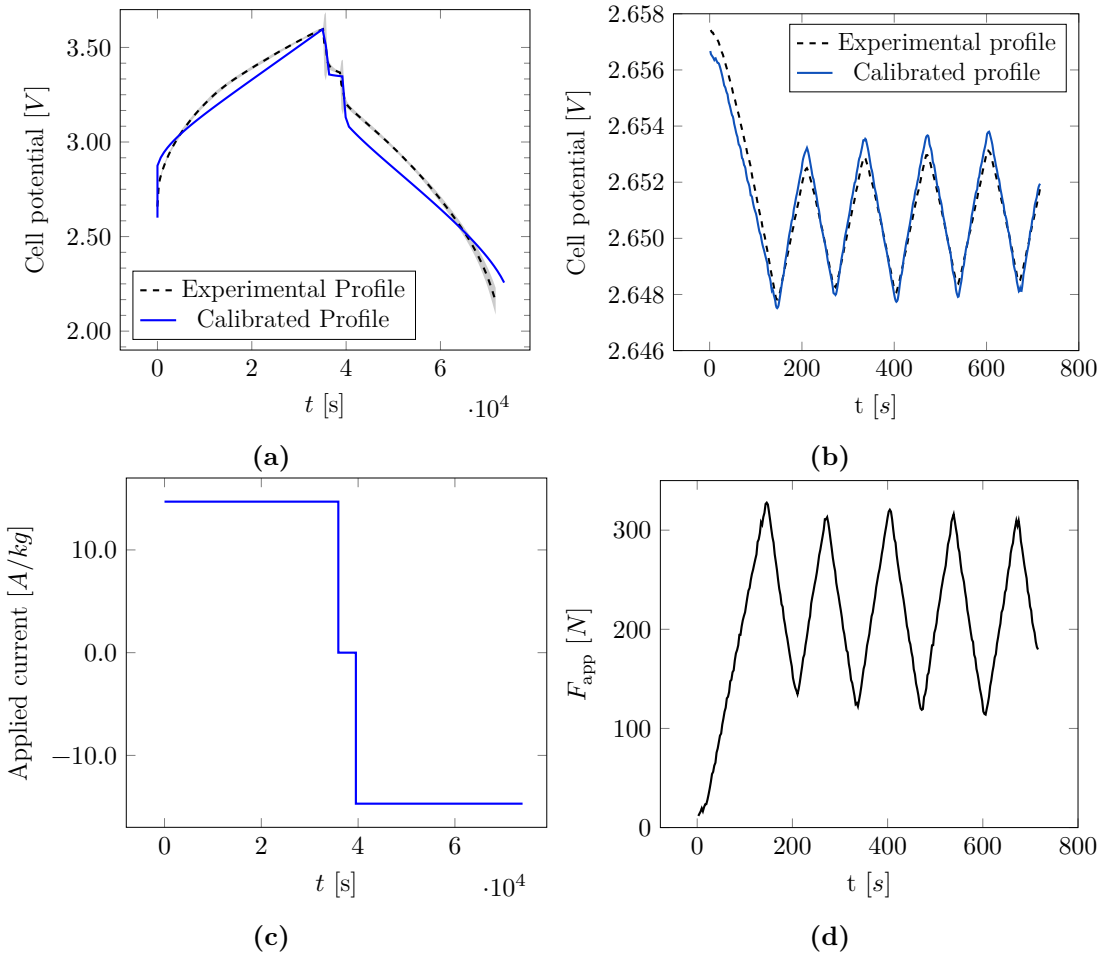

Figure 3.2: a) Experimental and calibrated voltage profiles at C/10 from **Paper D**. b) Experimental and calibrated voltage-strain coupling profiles from **Paper E**. c) Applied current profile for the charge-rest-discharge cycle at C/10, applicable to the response in (a). d) Applied force profile for the cell potential variation in (b).

4

Summary of papers

Paper A

Effects of lithium insertion induced swelling of a structural battery negative electrode
Carl Larsson, Fredrik Larsson, Johanna Xu, Kenneth Runesson, Leif E. Asp
Composites Science and Technology, 2023, 110299

In this paper, effects of lithiation of the carbon fibres on the mechanical properties and internal stress state of the negative electrode are studied. The method is outlined for analysis of features such as homogenized electrode stiffness and expansion, whereas the internal stress state analysis is carried out at the microscale using a synthetical representative volume element (RVE). In particular, two extreme cases representing a fully constrained and an unconstrained electrode are considered. High internal stresses are expected for the fully constrained RVE, while lower stresses are expected for the unconstrained RVE, where the RVE is allowed to expand freely. To properly represent geometrical change upon carbon fibre lithiation, finite deformation kinematics is adopted and a novel approach to homogeneous stress free expansion is presented. The numerical results show a significant difference in the computed internal stress state and homogenized tangent stiffness when comparing the proposed finite strain model against the equivalent model using linear (small strain) kinematics. Moreover, the computed homogeneous expansion of the negative electrode as a function of state of lithiation exhibits a trend that is similar to what is observed from experiments.

Paper B

Poro-mechanical analysis of a structural battery electrolyte: experimental study and model calibration
Carl Larsson, Fredrik Larsson, Ruben Tavano, Johanna Xu, Kenneth Runesson, Leif E. Asp
Mechanics of Materials, 2026, 105632

In this paper, the solid–fluid interaction within the structural battery electrolyte (SBE) is addressed through the application and validation of a continuum poro-viscoelastic model in the finite deformation setting. The model employs a Zener type rheology with a Norton evolution law to characterize the viscous response of the solid skeleton, which is coupled with a Darcy type seepage formulation to describe the transport of the liquid electrolyte. To calibrate the model, uniaxial compression tests are performed at varying strain rates on in-house manufactured cylindrical specimens. During these experiments, radial deformations are recorded using an optical camera, while mass measurements taken before and after compression provide a quantitative basis for the liquid electrolyte seepage. The model is further validated against independent stress relaxation tests. While discrepancies remain regarding time-dependent relaxation at high strain rates, the model successfully captures the rate-dependent stress–strain behaviour, radial extension, and fluid mass loss, particularly under large compressive strains.

Paper C

Mechanical response of the negative electrode in structural batteries with nonuniform microstructure
Carl Larsson, Ramesh Talreja, Fredrik Larsson, Richa Chaudhary, Amanda Persdotter, Leif E. Asp
Submitted

In this paper, the influence of manufacturing-induced nonuniform fibre distributions on the local stress state within the structural battery electrolyte (SBE) matrix is investigated. As carbon fibres expand during lithiation, the resulting reduction in inter-fibre distances generates compressive stresses in the SBE matrix that may lead to mechanical degradation. To quantify these effects, scanning electron microscopy (SEM) images of processed battery composites are utilized to obtain statistics on volume fraction and initial inter-fibre distances. A reconstruction procedure is employed to generate representative volume elements (RVEs), which are subsequently used in a boundary value problem. This analysis incorporates the

chemical expansion of the fibres and a poro-hyper-viscoelastic constitutive model for the SBE matrix. The results demonstrate that the extremes in local compressive stress are higher in the non-uniform microstructures compared to a reference model with a uniform hexagonal fibre pattern. The study thus highlights the importance of considering microstructural nonuniformity, stemming from the manufacturing process, when assessing the mechanical integrity and multifunctional performance of structural batteries.

Paper D

Electro-chemo-mechanical modelling of structural battery composite full cells
Carl Larsson, Fredrik Larsson, Johanna Xu, Kenneth Runesson, Leif E. Asp
npj Computational Materials, 2025, 141

In this paper, a coupled electro-chemo-mechanical modelling framework is proposed to enable the analysis of structural battery full cells. To support this framework, structural battery cells were manufactured in-house, providing experimental charge–rest–discharge voltage profiles for model calibration. A simplified continuum representation of the positive electrode is adopted, where redox reactions are represented using Butler–Volmer kinetics at the electrode interfaces. Mechanical stresses occur due to the lithiation-induced expansion of the carbon fibres in the negative electrode; however, the positive electrode is treated as stress-free. The measured model parameter values are employed where available, while the remaining parameters, primarily those governing the continuum positive electrode, are determined through parameter identification. This calibration utilizes experimental data obtained at different operating rates to ensure the model's ability to predict transient processes. A sensitivity analysis is performed to quantify the influence of each optimized parameter on the simulated cell voltage profiles and the associated cost function. The results demonstrate that, despite the simplified representation of the positive electrode, the model successfully captures the general trends of the experimental voltage profiles across varying rates. Finally, the framework is validated against independent experimental data from a separate cell, confirming its predictive capability for charge–rest–discharge processes.

Paper E

Electro-chemo-mechanical coupling in structural lithium-ion batteries: Experimental findings and numerical modelling
Rauan Al-Emrani, **Carl Larsson**, Clara Dahlberg, Fredrik Larsson, Leif E. Asp, Johanna Xu
Composites part B: Engineering, 2026, 113286

In this paper, the coupled electro-chemo-mechanical modelling framework is further developed to investigate the sensing capabilities of structural battery full cells. This work extends the previous formulation in **Paper D** by incorporating mechanical fields in all domains, allowing for the analysis of stresses in the entire cell volume. A key aspect of this development is the extension of the swelling behaviour and electro-chemo-mechanical coupling to the positive electrode, utilizing a homogenized continuum representation for a lithium iron phosphate (LFP) cathode on aluminium foil.

To support this framework, laminated cells were manufactured in-house to provide experimental data on voltage–strain coupling. By utilizing the extended model to interpret these results, the study identifies the carbon fibre negative electrode as the driver of the voltage–strain response. In contrast, the particle-based positive electrode exhibits a weak coupling. These findings provide a mechanistic understanding of interactions of mechanical stress and cell potential, and they demonstrate the predictive capabilities of the extended multiphysics framework.

5

Conclusions and outlook

The overall goal of the work presented in this thesis was to advance the understanding of coupled processes and develop improved computational tools for structural battery composites. Five sub-goals, as presented in Section 1.2 were identified, and have been fulfilled to varying degree of success.

Sub-goal 1: Characterize the mechanical response of the structural negative electrode during lithium insertion.

The foundation for mechanical analysis of the structural negative electrode was established in **Paper A**, which investigated the effects of carbon fibre lithiation within a finite strain setting. By accounting for concentration dependent fibre moduli as well as anisotropic expansion, the study characterized the evolution of internal stresses and the homogenized tangent stiffness of the electrode during lithiation. A central finding of this work is that the adoption of finite deformation kinematics is essential, whereas small strain models underestimate the magnitude of internal stresses during the lithiation process. Furthermore, a finite strain framework is necessary to consistently incorporate experimental observations of carbon fibre moduli, which were measured in the current configuration. The finite strain approach enables the computation of the effective increase in stress build-up as fibres expand within a macroscopically constrained composite. Conversely, the model predicts the effective expansion of the composite under unconstrained conditions.

While the model successfully established the necessary kinematic framework and quantified lithiation induced deformation in the SBE, it relied on an idealized uniform fibre arrangement and a simplistic material model for the SBE matrix. These simplifications provided incentives for further mechanical characterization and microstructural investigations conducted in **Papers B** and **C**.

Sub-goal 2: Propose and calibrate a constitutive model for the structural battery electrolyte (SBE) matrix.

This sub-goal was addressed in **Paper B**, which investigated the coupled solid–fluid interaction within the structural battery electrolyte. In this work, a Zener model was adopted for the solid skeleton, coupled with a Darcy-type seepage formulation to describe the transport of the liquid electrolyte. This framework was implemented within the finite deformation setting to capture the non-linear response of the SBE under operational loads, directly addressing the lack of matrix calibration identified in **Paper A**. The model was calibrated and validated against uniaxial compression and stress relaxation experiments. These tests were performed on in-house manufactured specimens. The experimental setup was restricted to uniaxial compression, which is well motivated since the primary stress state generated between fibres during expansion are of compressive nature.

With the proposed model, the rate-dependent behaviour, radial extension, and loss of fluid mass for test samples subjected to compression loads were successfully captured. To further refine this predictive tool, future work should focus on broadening the calibration space to include more stress states. Additionally, further refinement of the seepage model, and viscous evolution laws in the solid skeleton, can potentially lead to more accurate predictions of time-dependent stress relaxation, especially at high strain rates. In addition, incorporating deformation-dependent permeability through homogenization procedures allows for upscaling of transport properties as the pore geometry evolves with deformation.

Sub-goal 3: Investigate the influence of microstructural non-uniformity on the local stress fields.

The influence of nonuniformity in the fibre arrangement, inevitably arising from the manufacturing process, was addressed in **Paper C**. By utilizing SEM image informed RVE reconstructions, the study investigated how stochastic fibre arrangements affect local stress variations upon carbon fibre lithiation. The stresses in the RVE reconstructions were directly compared to those in a uniform hexagonal array fibre arrangement. This approach addresses the idealized arrangement limitation identified in **Paper A** by replacing idealized fibre arrangements with fibre arrangements that reflect the physical reality of the composite.

The results of the RVE reconstructions demonstrate that local compressive stresses are higher than those predicted by idealized models . This finding is significant, as it proves that uniform microstructural assumptions lead to an underestimation of internal stress peaks and, consequently, degradation risks.

While this work establishes a representation of the microstructure and the in-

ternal stress state, future research should focus on developing a characterization procedure for determining if, when, and how failure occurs in the inter-fibre spacing upon carbon fibre lithiation.

Sub-goal 4: Develop a fully coupled electro-chemo-mechanical model for a structural battery full cell.

This sub-goal was addressed in **Paper D**, which presents the transition to the device level through a fully coupled full cell model. To simulate galvanostatic charge-discharge cycles, a framework was established by adopting a simplified continuum representation for the positive electrode combined with non-linear Butler-Volmer kinetics. This integration allowed for the simultaneous analysis of ionic transport, chemical reactions and prediction of mechanical stresses in the negative electrode.

Through strategic calibration against experimental voltage profiles, the model reproduces charge-rest-discharge profiles at different charge rates well. A sensitivity analysis demonstrated that the ionic conductivity of the SBE is the primary factor that limits power performance. While the model successfully captures the fundamental electrochemical behaviour, the representation of the positive electrode remains rudimentary. Future work pertaining to **Paper D** should prioritize implementing a more sophisticated model for the positive electrode and evaluating the framework under a wider range of charge rates for further calibration and validation. Additionally, suitable experimental characterization related to interface conditions should be pursued in future work to further populate the model.

While the primary focus of this study was the electrochemical characteristics of the structural battery full cell, the mechanical response of all constituents requires deeper exploration. This is addressed in **Paper E**, where the model is extended to include mechanical considerations for all domains, enabling the calibration and investigation of critical multifunctional effects such as the voltage–strain coupling.

Sub-goal 5: Characterize the coupled potential-strain response (sensing) in the structural battery full cell.

The two-way coupling between mechanical loading and electric potential was explored in **Paper E** through an integrated experimental–computational approach. This study was designed to experimentally characterize the voltage–strain coupling effect in a structural battery full cell. By extending the electro-chemo-mechanical modelling framework in **Paper D** to include mechanical fields in all domains, we identified that the carbon fibre negative electrode is the primary contributor to the experimentally observed potential shifts. This finding provides evidence that the carbon fibres in the structural negative electrode possess an inherent sensing functionality. Moreover, we were able to calibrate the model parameters to fit the

observed voltage-strain behaviour very well.

The experimental evidence gathered here validates the multifunctional nature of the full cell. However, the tests were conducted in a discharged state, where the majority of the lithium remained hosted in the positive electrode. A progression of this study would be to characterize the voltage–strain coupling across different states of lithiation to determine how the voltage-strain coupling sensitivity evolves with state of charge. From a modelling perspective, there is a clear path toward up-scaling this micro-level framework to the laminate scale to investigate the effective coupling in a composite, with varied stacking orientations of structural battery laminates. Finally, implementing this fully coupled model within a finite deformation setting would allow for the integration of the fibre and SBE constitutive models from **Papers A** and **B**. This unification would enable studies on the effect of inhomogeneous lithiation of carbon fibres on the stresses in the SBE.

Bibliography

[1] E. D. Wetzel. Reducing weight: Multifunctional composites integrate power, communications, and structure. *AMPTIAC Quarterly*, 8(4):91–95, 2004.

[2] J. Snyder, E. Gienger, and E. Wetzel. Performance metrics for structural composites with electrochemical multifunctionality. *Journal of Composite Materials*, 49:1835–1848, 2015.

[3] R. F. Gibson. A review of recent research on mechanics of multifunctional composite materials and structures. *Composite Structures*, 92(12):2793–2810, 2010.

[4] A. Lendlein and R. S. Trask. Multifunctional materials: concepts, function-structure relationships, knowledge-based design, translational materials research. *Multifunctional Materials*, 1(1):010201, 2018.

[5] P. Ladpli, R. Nardari, F. Kopsaftopoulos, and F.-K. Chang. Multifunctional energy storage composite structures with embedded lithium-ion batteries. *Journal of Power Sources*, 414:517–529, 2019.

[6] K. Moyer et al. Carbon fiber reinforced structural lithium-ion battery composite: Multifunctional power integration for cubesats. *Energy Storage Materials*, 24:676–681, 2020.

[7] L. E. Asp, M. Johansson, G. Lindbergh, J. Xu, and D. Zenkert. Structural battery composites: A review. *Functional Composites and Structures*, 1:042001, 2019.

[8] L. E. Asp, K. Bouton, D. Carlstedt, S. Duan, R. Harnden, W. Johannisson, M. Johansen, M. K. G. Johansson, G. Lindbergh, F. Liu, K. Peuvot, L. M. Schneider, J. Xu, and D. Zenkert. A structural battery and its multifunctional performance. *Advanced Energy and Sustainability Research*, 2(3):2000093, 2021.

[9] J. Xu, Z. Geng, M. Johansen, D. Carlstedt, S. Duan, T. Thiringer, F. Liu, and L. E. Asp. A multicell structural battery composite laminate. *EcoMat*, 4(3):e12180, 2022.

[10] M. S. Siraj, S. Tasneem, D. Carlstedt, S. Duan, M. Johansen, C. Larsson, J. Xu, F. Liu, F. Edgren, and L. E. Asp. Advancing structural battery composites: Robust manufacturing for enhanced and consistent multifunctional performance. *Advanced Energy and Sustainability Research*, 4(11):2300109, 2023.

[11] R. Chaudhary, J. Xu, Z. Xia, and L. E. Asp. Unveiling the multifunctional carbon fiber structural battery (adv. mater. 48/2024). *Advanced Materials*, 36(48):2470382, 2024.

[12] R. Chaudhary, L. E. Asp, and V. Chaudhary. Redefining batteries as multifunctional materials. *Nature Reviews Materials*, 2026.

[13] International Energy Agency. Trends in electric car markets — global ev outlook 2025, 2025. Accessed: 2025-12-29.

[14] International Energy Agency. Trends in heavy-duty electric vehicles — global ev outlook 2025, 2025. Accessed: 2025-12-29.

[15] D. Carlstedt and L. E. Asp. Performance analysis framework for structural battery composites in electric vehicles. *Composites Part B: Engineering*, 186:107822, 2020.

[16] M. H. Kjell, E. Jacques, D. Zenkert, M. Behm, and G. Lindbergh. Pan-based carbon fiber negative electrodes for structural lithium-ion batteries. *Journal of The Electrochemical Society*, 158:A1455, 2011.

[17] M. H. Kjell, T. G. Zavalis, M. Behm, and G. Lindbergh. Electrochemical characterization of lithium intercalation processes of pan-based carbon fibers in a microelectrode system. *Journal of The Electrochemical Society*, 160:A1473–A1481, 2013.

[18] G. Fredi, S. Jeschke, A. Boulaoued, J. Wallenstein, M. Rashidi, F. Liu, R. Harnden, D. Zenkert, J. Hagberg, G. Lindbergh, P. Johansson, L. Stievano, and L. E. Asp. Graphitic microstructure and performance of carbon fibre li-ion structural battery electrodes. *Multifunctional Materials*, 1(1):015003, 2018.

[19] W. Johannisson et al. Multifunctional performance of a carbon fiber ud lamina electrode for structural batteries. *Composites Science and Technology*, 168:81–87, 2018.

[20] D. Zenkert, R. Harnden, L. E. Asp, G. Lindbergh, and M. Johansson. Multifunctional carbon fibre composites using electrochemistry. *Composites Part B: Engineering*, 273:111240, 2024.

[21] R. Tavano, J. Xu, C. Creighton, F. Liu, B. Dharmasiri, L. C. Henderson, and L. E. Asp. Influence of carbonisation temperatures on multifunctional properties of carbon fibres for structural battery applications. *Batteries & Supercaps*, 7(8):e202400110, 2024.

[22] E. Jacques, M. H. Kjell, D. Zenkert, G. Lindbergh, and M. Behm. Expansion of carbon fibres induced by lithium intercalation for structural electrode applications. *Carbon*, 59:246–254, 2013.

[23] S. Duan, A. H. Iyer, D. Carlstedt, F. Rittweger, A. Sharits, C. Maddox, K. R. Riemschneider, D. Mollenhauer, M. Colliander, F. Liu, and L. E. Asp. Effect of lithiation on the elastic moduli of carbon fibres. *Carbon*, 185:234–241, 2021.

[24] E. Jacques, G. Lindbergh, D. Zenkert, S. Leijonmarck, and M. H. Kjell. Piezoelectrochemical energy harvesting with lithium-intercalating carbon fibers. *ACS Applied Material Interfaces*, 7:13898–13904, 2015.

[25] R. Harnden, K. Peuvot, D. Zenkert, and G. Lindbergh. Multifunctional performance of sodiated carbon fibers. *Journal of The Electrochemical Society*, 165(13):B616, 2018.

[26] R. Harnden, D. Zenkert, and G. Lindbergh. Potassium-insertion in polyacrylonitrile-based carbon fibres for multifunctional energy storage, morphing, and strain-sensing. *Carbon*, 171:671–680, 2021.

[27] N. Ihrner, W. Johannisson, F. Sieland, D. Zenkert, and M. Johansson. Structural lithium ion battery electrolytes: Via reaction induced phase-separation. *Journal of Materials Chemistry A*, 5:25652–25659, 2017.

[28] L. M. Schneider, N. Ihrner, D. Zenkert, and M. Johansson. Bicontinuous electrolytes via thermally initiated polymerization for structural lithium ion batteries. *ACS Applied Energy Materials*, 2:4362–4369, 2019.

[29] M. Cattaruzza, Y. Fang, I. Furó, G. Lindbergh, F. Liu, and M. Johansson. Hybrid polymer-liquid lithium ion electrolytes: effect of porosity on the ionic and molecular mobility. *Journal of Materials Chemistry A*, 11:7006–7015, 2023.

[30] S. Duan, M. Cattaruzza, V. Tu, R. M. Auenhammer, R. Jänicke, M. K. G. Johansson, F. Liu, and L. E. Asp. Three-dimensional reconstruction and computational analysis of a structural battery composite electrolyte. *Communications Materials*, 4:49, 2023.

[31] V. Tu. *Computational Homogenization of Mechanical and Electro-Chemical Properties in Structural Battery Electrolytes.* Chalmers Tekniska Hogskola (Sweden), 2024.

[32] A. Pipertzis, J. Xu, N. Abdou, A. Martinelli, L. Asp, and J. Swenson. Ionic and electronic conductivity in structural negative electrodes. *Electrochimica Acta*, 512:145501, 2025.

[33] J. S. Sanchez, J. Xu, Z. Xia, J. Sun, L. E. Asp, and V. Palermo. Electrophoretic coating of lifepo4/graphene oxide on carbon fibers as cathode electrodes for structural lithium ion batteries. *Composites Science and Technology*, 208:108768, 2021.

[34] D. Carlstedt, K. Runesson, F. Larsson, V. Tu, R. Jänicke, and L. E. Asp. Computational modelling of structural batteries accounting for stress-assisted convection in the electrolyte. *International Journal of Solids and Structures*, 238:111343, 2022.

[35] D. Carlstedt, E. Marklund, and L. E. Asp. Effects of state of charge on elastic properties of 3d structural battery composites. *Composites Science and Technology*, 169:26–33, 2019.

[36] D. Carlstedt, K. Runesson, F. Larsson, J. Xu, and L. E. Asp. Electro-chemo-mechanically coupled computational modelling of structural batteries. *Multifunctional Materials*, 3:045002, 2020.

[37] D. Carlstedt, K. Runesson, F. Larsson, and L. E. Asp. On the coupled thermo–electro–chemo–mechanical performance of structural batteries with emphasis on thermal effects. *European Journal of Mechanics, A/Solids*, 94:104586, 2022.

[38] D. Grazioli, M. Magri, and A. Salvadori. Computational modeling of li-ion batteries. *Computational Mechanics*, 58:889–909, 2016.

[39] J. Newman and C. W. Tobias. Theoretical analysis of current distribution in porous electrodes. *Journal of the Electrochemical Society*, 109:1183, 1962.

[40] J. Newman and W. Tiedemann. Porous-electrode theory with battery applications. *AIChE Journal*, 21:25–41, 1975.

[41] A. Salvadori, E. Bosco, and D. Grazioli. A computational homogenization approach for li-ion battery cells: Part 1 - formulation. *Journal of the Mechanics and Physics of Solids*, 65:114–137, 2014.

[42] M. Doyle, T. F. Fuller, and J. Newman. Modeling of galvanostatic charge and discharge of the lithium/polymer/insertion cell. *Journal of the Electrochemical society*, 140(6):1526, 1993.

[43] M. Doyle and J. Newman. The use of mathematical modeling in the design of lithium/polymer battery systems. *Electrochimica Acta*, 40(13-14):2191–2196, 1995.

[44] D. Rollin, F. Larsson, K. Runesson, and R. Jänicke. Upscaling of chemo-mechanical properties of battery electrode material. *International Journal of Solids and Structures*, 281:112405, 2023.

[45] G. Bucci, Y. M. Chiang, and W. C. Carter. Formulation of the coupled electrochemical-mechanical boundary-value problem, with applications to transport of multiple charged species. *Acta Materialia*, 104:33–51, 2016.

[46] S. Qian, E. Cheng, O. Kakarelidis, S. Nguyen, M. Shaffer, A. Kucernak, A. Panesar, and E. S. Greenhalgh. Multiscale modelling of supercapacitors with hierarchical structure. *Journal of Power Sources*, 665:238956, 2026.

[47] C. Miehe, J. Schröder, and J. Schotte. Computational homogenization analysis in finite plasticity simulation of texture development in polycrystalline materials. *Computer Methods in Applied Mechanics and Engineering*, 171(3):387–418, 1999.

[48] M. G. Geers, V. G. Kouznetsova, and W. Brekelmans. Multi-scale computational homogenization: Trends and challenges. *Journal of computational and applied mathematics*, 234(7):2175–2182, 2010.

[49] N. P. van Dijk. Formulation and implementation of stress-driven and/or strain-driven computational homogenization for finite strain. *International Journal for Numerical Methods in Engineering*, 107:1009–1028, 2016.

[50] S. Saeb, P. Steinmann, and A. Javili. Aspects of Computational Homogenization at Finite Deformations: A Unifying Review From Reuss' to Voigt's Bound. *Applied Mechanics Reviews*, 68:050801, 2016.

[51] K. Terzaghi, R. B. Peck, and G. Mesri. *Soil mechanics in engineering practice*. John wiley & sons, 1996.

[52] S. Reese and S. Govindjee. A theory of finite viscoelasticity and numerical aspects. *International Journal of Solids and Structures*, 35(26):3455–3482, 1998.

[53] M. Landstorfer, S. Funken, and T. Jacob. An advanced model framework for solid electrolyte intercalation batteries. *Physical Chemistry Chemical Physics*, 13:12817–12825, 2011.